Chapter 4

Exergoeconomic investigation and multi-objective optimization of different ORC configurations for waste heat recovery

Organic Rankine cycles (ORCs) are one the widely used power cycles mostly suitable for low and medium-temperature heat sources. As discussed in Chapter 2, an ORC has four typical layouts. The simplest layout is known as the Basic ORC, and when a Basic ORC is coupled with an internal heat exchanger (IHE), the layout is known as a Recuperative ORC. Further, the Basic ORC with turbine bleeding is referred to as Regenerative ORC, and a Basic ORC that has both the IHE and turbine bleeding is referred to as Recuperative-Regenerative ORC (RR-ORC). Meanwhile, the first and second configurations of GT-based combined power and cooling systems discussed in Chapter 3 incorporated an R-ORC as one of the subsystems. As a matter of fact, R-ORC was arbitrarily chosen from the remaining ORC layouts for integration into the combined power and cooling systems. It presents a crucial opportunity to study the performance of the available ORC layouts, such that the best-performing ORC layout could be used in the earlier proposed combined systems. However, multiple comparative investigations have demonstrated that thermodynamically, modified ORCs outperform Basic ORC. But those studies were carried out considering fixed operating conditions of the ORC layouts. Moreover, the impact of modifications on the monetary aspect has not been studied yet. Based on the above research gaps, a multi-objective optimization-based comparative study of the ORC layouts is carried out in this chapter. The purpose of the aforementioned comparative study is

to replace the Recuperative ORC included in the combined power and cooling systems with the best-performing ORC configuration to improve the combined system's overall performance.

4.1 Description of the ORC layouts

Fig. 4.1(a) and Fig. 4.1(b) show the layout and the temperature-entropy (T-s) diagram of the Basic ORC. It comprises a vapour turbine (VT), a condenser (COND), a feed pump (FP) and a vapour generator (VG). The VG further includes the evaporator (EVA) and the economizer (ECO). The flue gas enters the VG and successively rejects heat at the EVA and the ECO. At the ECO, the heat is utilised for sensible heating of the organic fluid from the subcooled state to the liquid saturated state while EVA is the site of phase transformation. The saturated vapour expands in the VT up to the condenser pressure to produce power and drives the generator. After expansion in the VT, the vapour enters the COND where it gets converted to a saturated liquid by rejecting heat to the cooling water. The organic liquid is then fed to the VG by using a FP and this completes the cycle.

Fig. 4.2(a) and Fig. 4.2(b) show the layout and the T-s diagram of the Recuperative ORC. In this configuration, an IHE is used to recapture some amount of heat from the vapour exiting the VT. The recovered heat is then used to preheat the saturated liquid exiting the FP. The next is the Regenerative ORC that uses a feed heater (FH) where some fraction of vapour from the VT is extracted and mixed with the saturated liquid exiting the FP. The layout and the T-s diagram of the Regenerative ORC are shown in Fig. 4.3(a) and Fig. 4.3(b). The RR-ORC is the configuration that includes both the FH and the IHE. The vapour is first extracted from the VT and then it is mixed in the FH with the preheated saturated liquid exiting the FP. The preheating is done in the IHE by recapturing heat from the vapour exiting the VT. The layout and the T-s diagram of the RR-ORC are shown in Fig. 4.4(a) and Fig. 4.4(b).

4.2 Modelling

The current section first discusses the assumptions considered for modelling then the governing equations and the methodologies used for carrying out the multi-objective optimization-based exergoeconomic analysis of the ORC layouts are presented.

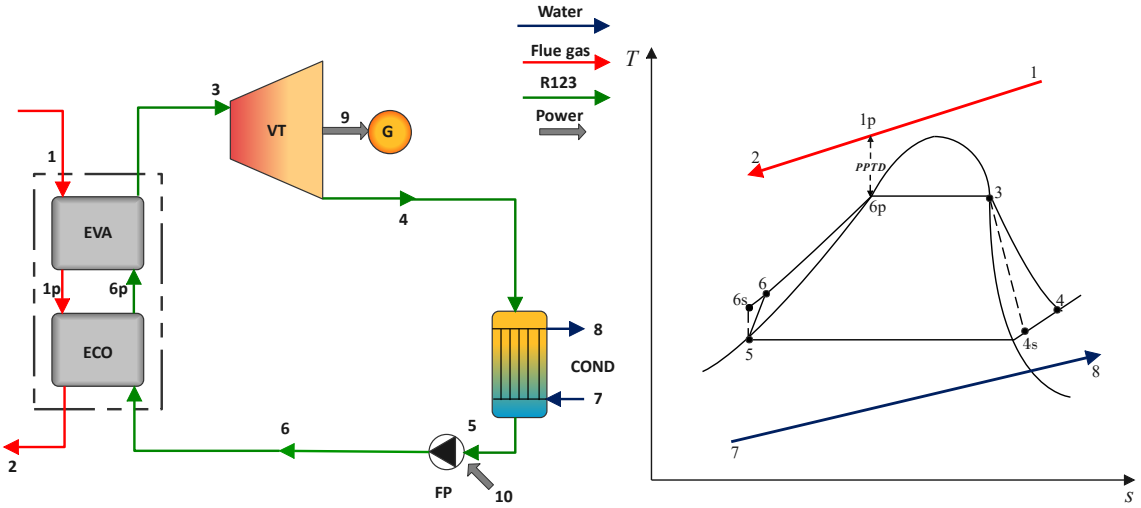

(a) Layout (b) T-s diagram

Fig. 4.1: Basic ORC.

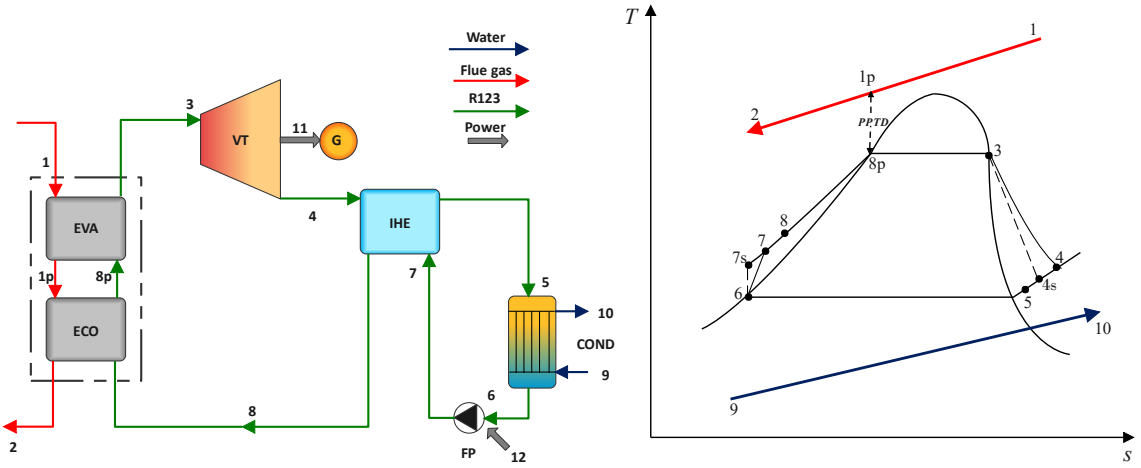

(a) Layout (b) T-s diagram

Fig. 4.2: Recuperative ORC.

4.2.1 Assumptions

The assumptions considered to simulate the ORC configurations are as follows [5]:

- Ambient temperature and pressure are 298.15 K and 101.3 kPa.
- The volumetric composition of the flue gas is considered as 75.07% N_2, 13.72% O_2, 3.14% CO_2, 2.97% H_2O (g) and 5.1% H_2O (l).
- The flow rate of the flue gas is 92.91 kg/s.
- Flue gas temperature and pressure at the VG inlet are 426 K and 104.3 kPa.
- The gas side pressure drop in the HRVG is assumed to be 3%.

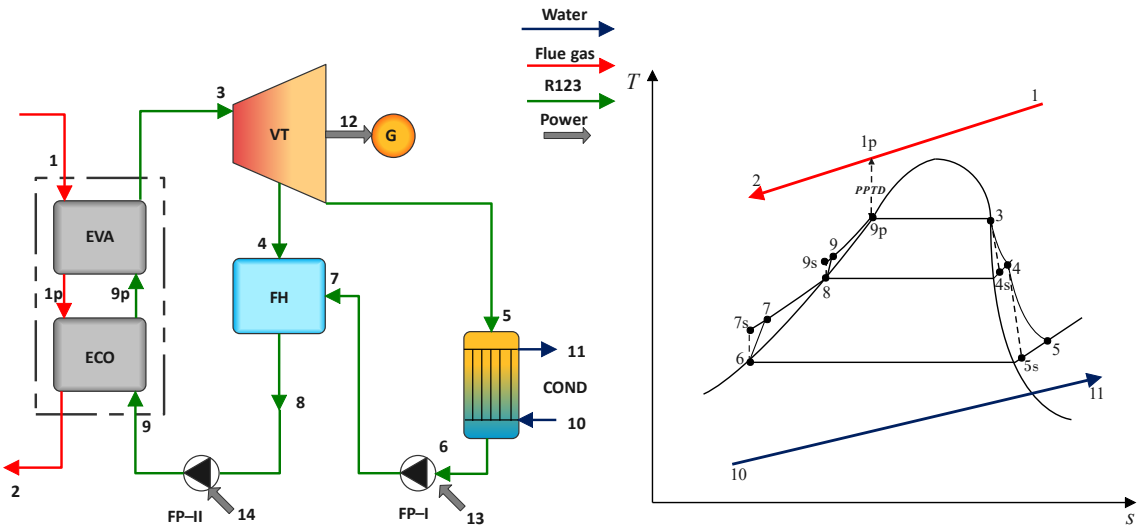

(a) Layout (b) T-s diagram

Fig. 4.3: Regenerative ORC.

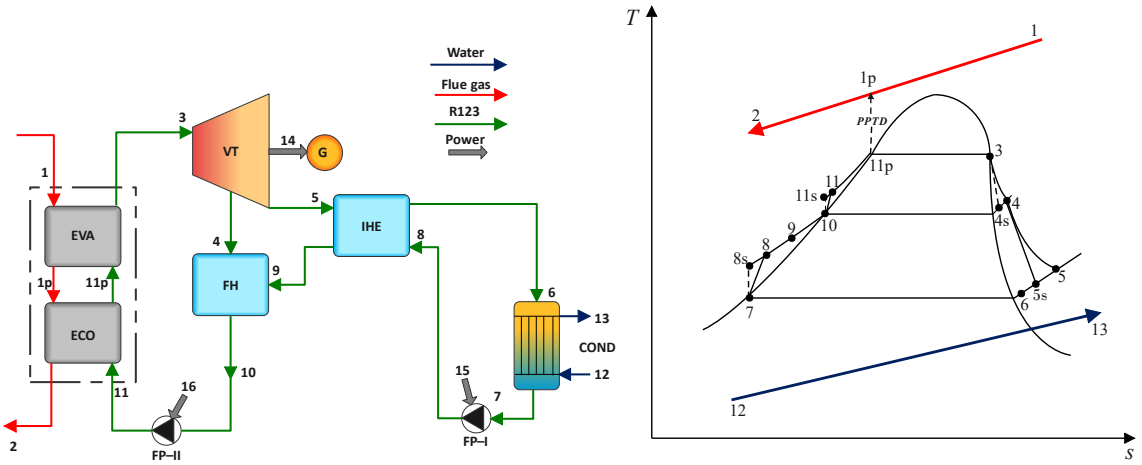

(a) Layout (b) T-s diagram

Fig. 4.4: RR-ORC.

- Isentropic efficiency of VT and FPs are 80% and 85%.
- The heat exchanger's effectiveness is 75%.
- The chemical exergy of the working fluid in the ORC is neglected.

Table 4.1 lists the base case working conditions considered for modelling the ORC configurations.

Table 4.1: The base case working conditions used for modelling the RR-ORC layouts [3].

Parameters	Symbols	Unit	Value
Evaporator temperature	T_3	K	340-400
Condenser temperature	T_7	K	304–308
Cooling water inlet temperature	T_{12}	K	298.15
Cooling water outlet temperature	T_{13}	K	302.15
Vapour extraction pressure	P_4	kPa	220
Pinch point temperature difference	ΔT_{pp}	K	281.15–293.15

4.2.2 Energy analysis

The enthalpy and entropy of the flue gas at the entry and exit of VG are calculated using the ideal gas mixture principle [5]. R123 was chosen as the operating medium for all four ORC configurations. REFPROP 9.0 [16] is used in the present work to evaluate the thermodynamic properties of R123 at various state points of ORC layouts. Further, in all four ORC configurations, the heat transfer between R123 and the flue gas is modelled using a PPTD in the range of 283.15-288.15 K [3]. The condition of R123 at the VT inlet and COND outlet are considered as saturated vapour and saturated liquid, respectively. The net power ($\dot{W}_{net}$) obtained from the ORCs is determined as follows [14]:

$$\dot{W}_{net} = \dot{W}_{VT} - \sum \dot{W}_{FP} \tag{4.1}$$

where $\dot{W}_{VT}$ is the power produced by the VT and $\dot{W}_{FP}$ is the work consumed by the FP.

The energy efficiency of the ORC can be determined using Eq. (4.2).

$$\eta_{sys} = \frac{\dot{W}_{net}}{\dot{Q}_{VG}} \tag{4.2}$$

where $\dot{Q}_{VG}$ is the heat recovered at the VG.

The energy balance equations for each component of the ORC layouts are presented in Table 4.2.

4.2.3 Exergy analysis

The exergy analysis of all four ORC configurations is performed by considering the same assumptions and correlations discussed in Chapter 3. The physical exergy of each stream of four ORC layouts is evaluated by using Eq. (3.23) whereas the

Table 4.2: Component-wise energy balance equations.

Components	Basic ORC	Recuperative ORC
VT	$\eta_s = (h_3 - h_4)/(h_3 - h_{4s})$	$\eta_s = (h_3 - h_4)/(h_3 - h_{4s})$
	$\dot{W} = \dot{m}_r(h_3 - h_4)$	$\dot{W} = \dot{m}_r(h_3 - h_4)$
IHE	-	$\dot{Q} = \dot{m}_r(h_4 - h_5)$
	-	$(h_4 - h_5) = (h_8 - h_7)$
COND	$\dot{Q} = \dot{m}_r(h_4 - h_5)$	$\dot{Q} = \dot{m}_r(h_5 - h_6)$
	$\dot{m}_r(h_4 - h_5) = \dot{m}_w(h_8 - h_7)$	$\dot{m}_r(h_5 - h_6) = \dot{m}_w(h_10 - h_9)$
FP	$\eta_s = (h_{6s} - h_5)/(h_6 - h_5)$	$\eta_s = (h_{7s} - h_6)/(h_7 - h_6)$
	$\dot{W} = \dot{m}_r(h_6 - h_5)$	$\dot{W} = \dot{m}_r(h_7 - h_6)$
VG	$\dot{m}_r(h_3 - h_{6p}) = \dot{m}_g(h_1 - h_{1p})$	$\dot{m}_r(h_3 - h_{8p}) = \dot{m}_g(h_1 - h_{1p})$
	$\dot{m}_r(h_{6p} - h_6) = \dot{m}_g(h_{1p} - h_2)$	$\dot{m}_r(h_{9p} - h_9) = \dot{m}_g(h_{1p} - h_2)$
Components	**Regenerative ORC**	**RR-ORC**
VT	$\eta_s = (h_3 - h_4)/(h_3 - h_{4s})$	$\eta_s = (h_3 - h_4)/(h_3 - h_{4s})$
	$\eta_s = (h_4 - h_5)/(h_4 - h_{5s})$	$\eta_s = (h_4 - h_5)/(h_4 - h_{5s})$
	$\dot{W} = \dot{m}_r[(h_3 - h_4) + x(h_4 - h_5)]$	$\dot{W} = \dot{m}_r[(h_3 - h_4) + x(h_4 - h_5)]$
IHE	-	$\dot{Q} = \dot{m}_r(h_5 - h_6)$
	-	$(h_5 - h_6) = (h_9 - h_8)$
FH	$\dot{Q} = \dot{m}_r h_8$	$\dot{Q} = \dot{m}_r h_{10}$
	$xh_9 + (1 - x)h_4 = h_{10})$	$xh_7 + (1 - x)h_4 = h_8)$
COND	$\dot{Q} = \dot{m}_r(h_5 - h_6)$	$\dot{Q} = \dot{m}_r(h_6 - h_7)$
	$\dot{m}_r(h_5 - h_6) = \dot{m}_w(h_{11} - h_{10})$	$\dot{m}_r(h_6 - h_7) = \dot{m}_w(h_{13} - h_{12})$
FP-I	$\eta_s = (h_{7s} - h_6)/(h_7 - h_6)$	$\eta_s = (h_{8s} - h_7)/(h_8 - h_7)$
	$\dot{W} = \dot{m}_r(h_7 - h_6)$	$\dot{W} = \dot{m}_r(h_8 - h_7)$
FP-II	$\eta_s = (h_{8s} - h_7)/(h_8 - h_7)$	$\eta_s = (h_{11s} - h_{10})/(h_{11} - h_{10})$
	$\dot{W} = \dot{m}_r(h_8 - h_7)$	$\dot{W} = \dot{m}_r(h_{11} - h_{10})$
VG	$\dot{m}_r(h_3 - h_{9p}) = \dot{m}_g(h_1 - h_{1p})$	$\dot{m}_r(h_3 - h_{11p}) = \dot{m}_g(h_1 - h_{1p})$
	$\dot{m}_r(h_{9p} - h_9) = \dot{m}_g(h_{1p} - h_2)$	$\dot{m}_r(h_{11p} - h_{11}) = \dot{m}_g(h_{1p} - h_2)$

chemical exergy of the flue gas is calculated using Eq. (3.24). Lastly, the exergy destruction rate and exergy efficiency for each component is determined by using Eq. (3.28) and Eq. (3.29), respectively. Meanwhile, the exergy balance equations for the ORC layouts are displayed in Table 4.3. Moreover, the exergy efficiency of the overall system for all four ORC configurations in the present is calculated by using Eq. (4.3) [5].

$$\varepsilon_{sys} = \frac{\dot{W}_{net}}{\dot{E}_1 - \dot{E}_2} \tag{4.3}$$

Table 4.3: Component-wise exergy balance equations.

Components	Basic ORC	Recuperative ORC
VT	$\dot{E}_3 = \dot{E}_4 + \dot{E}_9 + \dot{E}_{10} + \dot{E}_D$	$\dot{E}_3 = \dot{E}_4 + \dot{E}_{11} + \dot{E}_{12} + \dot{E}_D$
IHE	-	$\dot{E}_4 + \dot{E}_7 = \dot{E}_5 + \dot{E}_8 + \dot{E}_D$
COND	$\dot{E}_4 + \dot{E}_7 = \dot{E}_5 + \dot{E}_8 + \dot{E}_D$	$\dot{E}_5 + \dot{E}_9 = \dot{E}_6 + \dot{E}_{10} + \dot{E}_D$
FP	$\dot{E}_5 + \dot{E}_{10} = \dot{E}_6 + \dot{E}_D$	$\dot{E}_6 + \dot{E}_{12} = \dot{E}_7 + \dot{E}_D$
VG	$\dot{E}_1 + \dot{E}_6 = \dot{E}_2 + \dot{E}_3 + \dot{E}_D$	$\dot{E}_1 + \dot{E}_8 = \dot{E}_2 + \dot{E}_3 + \dot{E}_D$
Components	Regenerative ORC	RR-ORC
VT	$\dot{E}_3 = \dot{E}_4 + \dot{E}_5 + \dot{E}_{12} + \dot{E}_{13} + \dot{E}_{14} + \dot{E}_D$	$\dot{E}_3 = \dot{E}_4 + \dot{E}_5 + \dot{E}_{12} + \dot{E}_{15} + \dot{E}_{16} + \dot{E}_D$
IHE	-	$\dot{E}_5 + \dot{E}_8 = \dot{E}_6 + \dot{E}_9 + \dot{E}_D$
COND	$\dot{E}_5 + \dot{E}_{10} = \dot{E}_6 + \dot{E}_{11} + \dot{E}_D$	$\dot{E}_6 + \dot{E}_{12} = \dot{E}_7 + \dot{E}_{13} + \dot{E}_D$
FP-I	$\dot{E}_6 + \dot{E}_{13} = \dot{E}_7 + \dot{E}_D$	$\dot{E}_7 + \dot{E}_{15} = \dot{E}_8 + \dot{E}_D$
FP-II	$\dot{E}_8 + \dot{E}_{14} = \dot{E}_9 + \dot{E}_D$	$\dot{E}_{10} + \dot{E}_{16} = \dot{E}_{11} + \dot{E}_D$
FH	$\dot{E}_4 + \dot{E}_7 = \dot{E}_8 + \dot{E}_D$	$\dot{E}_4 + \dot{E}_9 = \dot{E}_{10} + \dot{E}_D$
VG	$\dot{E}_1 + \dot{E}_9 = \dot{E}_2 + \dot{E}_3 + \dot{E}_D$	$\dot{E}_1 + \dot{E}_{11} = \dot{E}_2 + \dot{E}_3 + \dot{E}_D$

4.2.4 Exergoeconomic analysis

In this study, the specific exergy costing (SEPCO) [2] method is used to perform the exergoeconomic analysis of the ORC layouts. The first step in this method is to evaluate all exergy flow rates crossing a component's control surface, followed by the proper description of the fuel, product, and loss components of exergy. The cost rate is then applied to all the exergy streams using the following cost balance equation [17]:

$$\sum_{e} \dot{C}_{e,k} + \dot{C}_{work,k} = \dot{C}_{heat,k} + \sum_{i} \dot{C}_{i,k} + \dot{Z}_k \tag{4.4}$$

where $\dot{C}$ is the cost flow rate in \$/h, which can be defined in terms of exergy flow rate and cost per unit of exergy (c_i) as follows [17]:

$$\dot{C}_i = c_i \times \dot{E}_i \tag{4.5}$$

In Eq. (4.4), $\dot{Z}_k$ is the capital cost rate which is the sum of capital investment cost, and operating and maintenance cost incurred by the component k per hour. $\dot{Z}_k$ is calculated by using the following relation [22]:

$$\dot{Z}_k = \frac{PEC_k \times CRF \times \phi}{N} \tag{4.6}$$

where PEC_k stands for purchase equipment cost of the component k in US dollars, N is the annual service hours, and ϕ is the maintenance factor [13]. CRF is the

capital recovery factor evaluated using the following relation [10].

$$CRF = \frac{j \times (1+j)^n}{(1+j)^n - 1} \tag{4.7}$$

where j is the interest rate [1] and n is the service life of the components [15]. The values of the exergoeconomic input parameters used in Eq. (4.6) and Eq. (4.7) are provided in Table 4.4.

Table 4.4: The exergoeconomic input parameters.

Parameters	Unit	Values	Ref.
Annual service hours (N)	h	7446	[13]
Maintenance factor (ϕ)	-	1.06	[13]
Interest rate (j)	%	12	[1]
Service life (n)	years	20	[15]

The most detailed and accurate information on PEC_k can be found from the manufacturers of specific equipment. The PEC_k can also be expressed in terms of mathematical functions of important operating parameters, which is a useful and helpful technique. The mathematical functions reported in the literature are used in this chapter to evaluate PEC_k of all the components of the ORC layouts. The mathematical functions, however, are developed in various years, thus Eq. (4.8) [4] is used to update the costs from the original year to the reference year (2022).

$$PEC_{k,ref} = PEC_{k,org}\left(\frac{CI_{ref}}{CI_{org}}\right) \tag{4.8}$$

where CI_{ref} and CI_{org} are the cost index for the reference year and original year, respectively.

For each component of the ORC layouts, the mathematical functions are given in Table 4.5 along with the corresponding original year and associated cost indices. The cost index of the reference year is considered as 1773.3 [12]. Meanwhile, the heat transfer areas of the VG and the IHE used in respective mathematical functions are calculated by assuming those as shell and tube heat exchangers. The methodology for modelling the shell and tube heat exchangers reported in Ref. [21] is implemented in this study.Thereafter, the cost balance equations are developed with the aid of the auxiliary equations and appropriate assumptions. Then the cost balance equations give a system of linear equations which are solved by using the matrix inversion method [6]. The cost balance and the auxiliary equations developed for the ORC layouts are given in Table 4.6. Besides, the cost flow rate ($\dot{C}_1$) for the flue gas

entering the VG is considered as 150 \$/h based on the Ref. [5].

Table 4.5: The correlations used in calculation of the purchased equipment costs.

Components	PEC_k	Original year	CI_{org}
VT	$6000(\dot{W}_{VT}^{0.7})$	2013 [4]	1552.8
IHE	$1.3(190 + 310A_{IHE})$	2010 [4, 12]	1446.5
COND	$177(\dot{m}_r)$	2011 [4, 12]	1476.7
FP	$3540(\dot{W}_{FP}^{0.71})$	2011 [4, 12]	1476.7
VG	$309.143(A_{VG}) + 231.915$	2006 [4, 12]	1274.8
FH	$(527.7/397)^{1.7} \times \acute{C}$	2003 [4, 12]	1552.8
	$\log_{10}\acute{C} = 4.20 - 0.204\log_{10}\dot{V} + 0.1245(\log_{10}\dot{V})^2$		

Table 4.6: The cost equations formulated for the ORC layouts.

Components	Basic ORC	Recuperative ORC
VT	$\dot{C}_3 + \dot{Z} = \dot{C}_4 + \dot{C}_9 + \dot{C}_{10}$	$\dot{C}_3 + \dot{Z} = \dot{C}_4 + \dot{C}_{11} + \dot{C}_{12}$
	$c_3 = c_4, c_9 = c_{10}$	$c_3 = c_4, c_{11} = c_{12}$
IHE	-	$\dot{C}_4 + \dot{C}_7 + \dot{Z} = \dot{C}_5 + \dot{C}_8$
	-	$c_4 = c_5$
COND	$\dot{C}_4 + \dot{C}_7 + \dot{Z} = \dot{C}_5 + \dot{C}_8$	$\dot{C}_5 + \dot{C}_9 + \dot{Z} = \dot{C}_6 + \dot{C}_{10}$
	$c_7 = 0, c_4 = c_5$	$c_9 = 0, c_5 = c_6$
FP	$\dot{C}_5 + \dot{C}_{10} + \dot{Z} = \dot{C}_6$	$\dot{C}_6 + \dot{C}_{12} + \dot{Z} = \dot{C}_7$
VG	$\dot{C}_1 + \dot{C}_6 + \dot{Z} = \dot{C}_2 + \dot{C}_3$	$\dot{C}_1 + \dot{C}_8 + \dot{Z} = \dot{C}_2 + \dot{C}_3$
	$\dot{C}_1 = 150, c_1 = c_2$	$\dot{C}_1 = 150, c_1 = c_2$
Components	Regenerative ORC	RR-ORC
VT	$\dot{C}_3 + \dot{Z} = \dot{C}_4 + \dot{C}_5 + \dot{C}_{12} + \dot{C}_{13} + \dot{C}_{14}$	$\dot{C}_3 + \dot{Z} = \dot{C}_4 + \dot{C}_5 + \dot{C}_{12} + \dot{C}_{15} + \dot{C}_{16}$
	$c_3 = c_4, c_3 = c_5, c_{12} = c_{13}, c_{12} = c_{14}$	$c_3 = c_4, c_3 = c_5, c_{12} = c_{15}, c_{12} = c_{16}$
IHE	-	$\dot{C}_5 + \dot{C}_8 + \dot{Z} = \dot{C}_6 + \dot{C}_9$
	-	$c_5 = c_6$
COND	$\dot{C}_5 + \dot{C}_{10} + \dot{Z} = \dot{C}_6 + \dot{C}_{11}$	$\dot{C}_6 + \dot{C}_{12} + \dot{Z} = \dot{C}_7 + \dot{E}_C$
	$c_{10} = 0, c_5 = c_6$	$c_{12} = 0, c_6 = c_7$
FP-I	$\dot{C}_6 + \dot{C}_{13} + \dot{Z} = \dot{C}_7$	$\dot{C}_7 + \dot{C}_{15} + \dot{Z} = \dot{C}_8$
FP-II	$\dot{C}_8 + \dot{C}_{14} + \dot{Z} = \dot{C}_9$	$\dot{C}_{10} + \dot{C}_{16} + \dot{Z} = \dot{C}_{11}$
FH	$\dot{C}_4 + \dot{C}_7 + \dot{Z} = \dot{C}_8$	$\dot{C}_4 + \dot{C}_9 + \dot{Z} = \dot{C}_{10}$
VG	$\dot{C}_1 + \dot{C}_9 = \dot{C}_2 + \dot{C}_3$	$\dot{C}_1 + \dot{C}_{11} = \dot{C}_2 + \dot{C}_3$
	$\dot{C}_1 = 150, c_1 = c_2$	$\dot{C}_1 = 150, c_1 = c_2$

The cost flow rates at each state point of the four ORC configurations are determined by solving the cost balance equations and further, the cost per unit of exergy (c_k) is also calculated to evaluate exergoeconomic parameters. These parameters are the exergoeconomic factor (f_k), relative cost difference (r_k), cost per unit of product exergy ($c_{P,k}$), cost per unit of fuel exergy ($c_{F,k}$) and the cost associated with the ex-

ergy destruction ($\dot{C}_{D,k}$) and the exergy loss ($\dot{C}_{L,k}$). The $c_{F,k}$ is defined as the average cost of each unit of exergy delivered to the k^{th} component. Similarly, $c_{P,k}$ is defined as the average cost at which k^{th} component generates each unit of exergy. The $\dot{C}_{D,k}$ is the economic loss related to the loss of exergy owing to the irreversibility of the system component. The $\dot{C}_{L,k}$, on the other hand, measures the economic loss caused by the loss of exergy from the system to the environment. Meanwhile, r_k is the rate of increase in the cost per unit of product exergy compared to the cost per unit of fuel exergy. Finally, f_k determines the relative significance of exergy-related costs (exergy destruction and exergy loss) and non-exergy-related costs (capital cost) in a component. These parameters are calculated by applying Eqs. (4.9) to (4.14) [5].

$$c_{F,k} = \frac{\dot{C}_{F,k}}{\dot{E}_{F,k}} \tag{4.9}$$

$$c_{P,k} = \frac{\dot{C}_{P,k}}{\dot{E}_{P,k}} \tag{4.10}$$

$$\dot{C}_{D,k} = c_{F,k}\dot{E}_{D,k} \tag{4.11}$$

$$\dot{C}_{L,k} = c_{F,k}\dot{E}_{L,k} \tag{4.12}$$

$$r_k = \frac{c_{P,k} - c_{F,k}}{c_{F,k}} \tag{4.13}$$

$$f_k = \frac{\dot{Z}_k}{\dot{Z}_k + \dot{C}_{D,k} + \dot{C}_{L,k}} \tag{4.14}$$

Finally, the total system cost rate is evaluated by using Eq. (4.15) [5]:

$$\dot{C}_{sys} = \sum_k \dot{Z}_k + \sum_k \dot{C}_{D,k} + \dot{C}_{L,k} \tag{4.15}$$

4.2.5 Multi-objective optimization

In the present study, a Pareto envelope-based selection algorithm-II (PESA-II) [9] is used to perform the multi-objective optimization on the ORC configurations. PESA-II is an updated version of PESA that was introduced by Corne et al. [8] in the year 2000. PESA uses the hyper-gride crowding scheme for selection and diversity maintenance. In addition to the internal population, it also uses an external population known as an archive. Random solutions are used to populate the internal population, and the archive is initialized as an empty set. The internal population is subjected to non-dominated sorting while allocating the best non-dominated members to the archive. If the pre-existing members of the archive dominate the

transferred members, then they are rejected. The process continues and once the terminating condition is met, the transition of non-dominated members to the archive is stopped. Otherwise, the current internal population members are removed, and the procedure is repeated. The selection process in the original PESA was particle-based due to which it suffered from inadequate spread of the Pareto fronts. Corne et al. [8] addressed this limitation by integrating the concept of hyperbox allocation into the objective space and using region-based selection instead of particle-based. Fig. A.1 (refer to Appendix) presents a flowchart that describes the fundamental operation of PESA-II.

In a recent article [18], while comparing three different multi-objective evolutionary algorithms for exergoenvironomic optimization of a benchmark CHP system, PESA-II was found to have a high degree of convergence and diversity, as well as a low computational time over NSGA-II and SPEA-II. Therefore, PESA-II is used in this study to perform multi-objective optimization. The PESA-II routine is linked to an in-house built MATLAB code that simulates the exergoeconomic performance of the ORC configurations. For a given set of decision variables, it then returns the Pareto optimal solutions while optimizing both objectives simultaneously, based on the number of equality/inequality constraints. The mathematical model for the current multi-objective optimization problem is as given below [11]:

$$\begin{cases} x = (T_{EVA}, T_{COND}, \text{PPTD})^T \\ f = (f_1(\varepsilon_{sys}), f_2(\dot{C}_{sys}))^T \\ g_j(x) \leq 0 \colon \forall j = \text{EVA}, \text{COND}, \text{PPTD} \\ 340\text{K} \leq T_{EVA} \leq 400\text{K} \\ 304\text{K} \leq T_{COND} \leq 308\text{K} \\ 281.15\text{K} \leq \text{PPTD} \leq 293.15\text{K} \end{cases} \tag{4.16}$$

As can be seen in Eq. (4.16), the objective functions in this optimization problem are the exergy efficiency (ε_{sys}) and the system cost rate ($\dot{C}_{sys}$). This study aims to maximize ε_{sys} and minimize $\dot{C}_{sys}$, subject to a set of inequality constraints signifying the thermodynamic limitations that exist during the heat transfer process occurring in the heat exchangers such as IHE and the VG. These constraints are formulated based on Ref. [20]. Hence, one more additional constraint; $T_2 \leq 373$ K, is also considered. The decision variables considered for the multi-objective optimization are the evaporator temperature (T_{EVA}), condenser temperature (T_{COND}), and PPTD.

In Eq. (4.16), the decision variables are given with their corresponding upper and lower limits. These limits are selected based on Ref. [3] with proper adjustments to suit the current ORC models in consideration. The lower limit of T_{COND} is taken as 304 K to maintain a small terminal temperature differential between the temperature of condensate and R123 in the condenser. The lower limit of the PPTD is considered 381.5 K to restrict the temperature of the flue gas leaving the VG above 100 °C to prevent acid formation at the economizer section. The other user-defined parameters implemented for executing the optimization algorithm (PESA-II) are given in Table 4.7. The crossover and mutation probabilities are chosen based on Ref. [9] while the other parameters are selected following Ref. [8]. It is important to note that, like most evolutionary algorithms, PESA-II does not guarantee to find global optimal solutions in the Pareto fronts. However, one thing can be ensured that all the optimal solutions are the best trade-off solution.

Table 4.7: The parameter settings used for executing PESA-II [8, 9].

Parameters	Value
Population size	100
Archive size	100
Crossover probability	0.7
Mutation probability	0.3
Number of iterations	50

Further, in this study, the Technique for Order Preference by Similarity to an Ideal Solution (TOPSIS) [7] is used to obtain the final optimal solution from the Pareto fronts. The first step in the TOPSIS decision-maker is to construct the decision matrix of order n by m, where n is the number of members (solutions) and, m is the number of criteria (objectives), as shown in Eq. (4.17).

$$D = \begin{array}{c} \begin{matrix} \mathrm{C}_1 & \mathrm{C}_2 & \mathrm{C}_3 & \dots & \mathrm{C}_n \end{matrix} \\ \begin{bmatrix} x_{11} & x_{12} & x_{13} & \dots & x_{1n} \\ x_{21} & x_{22} & x_{23} & \dots & x_{2n} \\ x_{31} & x_{32} & x_{33} & \dots & x_{3n} \\ \vdots & \vdots & \vdots & \ddots & \vdots \\ x_{m1} & x_{m2} & x_{m3} & \dots & x_{mn} \end{bmatrix} \end{array} \begin{matrix} \mathrm{A}_1 \\ \mathrm{A}_2 \\ \mathrm{A}_3 \\ \vdots \\ \mathrm{A}_n \end{matrix} \tag{4.17}$$

where $A_1, A_2, .., A_m$ are the number of alternative, $C_1, C_2, .., C_n$ are the number of

criteria and x_{ij} is the element of alternative A_i under criteria C_j.

The weights assigned to each criterion can be defined in form of a row matrix with the dimension of $1 \times n$ as shown below:

$$W = \begin{bmatrix} w_1 & w_2 & w_3 & \dots & w_n \end{bmatrix} \tag{4.18}$$

where w_j is the weight of criterion C_j. The weights are equivalent to the priority assigned to the criteria on a scale of 0 to 1 ($\sum_{j=1}^{n} w_j = 1$).

Evaluation criteria can be classified into two categories: cost and benefit. The benefit criterion prioritizes higher value, while the cost criterion does the opposite. The decision matrix requires normalization to convert the diverse dimensions of the elements into non-dimensional, enabling comparison between the criteria. This is achieved using the following correlation:

$$p_{ij} = \frac{x_{ij}}{\sum_{i=1}^{m} x_{ij}} \tag{4.19}$$

The normalized decision matrix (P) can then be shown as follows:

$$P = (p_{ij})_{m \times n} \tag{4.20}$$

Then for each criterion, the ideal best solution (I^+) matrix and ideal worst solution (I^-) matrix are determined as follows:

$$I^+ = (p_1^+, p_2^+, ...P_m^+) \tag{4.21}$$

$$I^- = (p_1^-, p_2^-, ...P_m^-) \tag{4.22}$$

where

$$p_j^+ = \{\max p_{ij}\} \tag{4.23}$$

$$p_j^- = \{\min p_{ij}\} \tag{4.24}$$

Then the performance vector (PV_i) is evaluated using the following equation:

$$PV_i = \frac{E_i^-}{E_i^+ + E_i^-} \tag{4.25}$$

where E_i^+ and E_i^- are the Euclidean distance of each alternative from the ideal best

solution (p_j^+) and the ideal worst solution (p_j^-), calculated as follows:

$$E_i^+ = \sqrt{\sum_{j=0}^{n} w_j \left(p_{ij} - p_j^+\right)} \tag{4.26}$$

$$E_i^- = \sqrt{\sum_{j=0}^{n} w_j \left(p_{ij} - p_{j-}^-\right)} \tag{4.27}$$

where $i = 1, 2, 3 \ldots, m$ and $j = 1, 2, 3 \ldots, n$.

Then elements of PV_i are sorted in order of decreasing values and ranks are given based on that order. The optimal solution corresponding to the first ranked element is chosen as the best optimal solution.

4.3 Results and discussions

4.3.1 Model validation

The ORC models are verified by comparing several key performance indicators with the results of other identical systems operating under the same conditions as those stated in Ref. [19]. The validation results for each of the four configurations are displayed in Table 4.8. As can be observed, the parameters used for comparison have a relative error of less than 3%, ensuring that the current models are in good agreement with those found in Ref. [19].

Table 4.8: Model validation of the ORC layouts with those of Ref. [19].

Basic ORC				Recuperative ORC		
Parameters	Ref. [19]	Present work	Error (%)	Ref. [19]	Present work	Error (%)
$\dot{W}_{net}$	49.04	49.64	1.22	54.30	55.01	1.30
η_{sys}	19.46	19.70	1.23	21.5	21.83	1.53
$\dot{E}_D$	50.92	52.41	2.92	49.50	48.28	2.86
Regenerative ORC				RR-ORC		
Parameters	Ref. [19]	Present work	Error (%)	Ref. [19]	Present work	Error (%)
$\dot{W}_{net}$	55.53	56.55	1.83	57.54	58.84	2.25
η_{sys}	22.00	22.44	2.00	22.83	23.3	2.05
$\dot{E}_D$	47.30	46.38	1.94	42.20	43.20	2.36

4.3.2 Parametric results

The parametric analysis aims to determine the impact of crucial decision variables such as the evaporator temperature (T_{EVA}), condenser temperature (T_{COND}), and PPTD on the exergy efficiency and the system cost rate of the ORC configurations. It is carried out by varying the decision variables one by one while keeping the rest of the variables fixed at the base case condition.

Effect of evaporator temperature

The impact of raising the evaporator temperature on the exergy efficacy of the four ORC layouts is depicted in Fig. 4.5(a). It is observed that the exergy efficiency of all four layouts first rises and peaks before beginning to fall. The exergy efficiency of the Basic ORC reaches its maximum value at T_{EVA}=380 K, whereas for the remaining layouts, exergy efficiency reaches its maximum value at T_{EVA}=385 K. The Basic ORC, Recuperative ORC, Regenerative ORC, and RR-ORC have maximum efficiency values of 43.26%, 47.63%, 48.81%, and 49.94%, respectively. Up until T_{EVA} reaches the threshold value corresponding to the peak efficiency, both the VT and the FP work increase. Thereafter, the FP work predominates and the exergy efficiency drops. Additionally, Fig. 4.5(a) demonstrates that, in comparison to the others, the efficiency of the RR-ORC is maximum over the entire range of T_{EVA}, but it is minimum over the same range for the Basic ORC.

The impact of T_{EVA} on the system cost rate for each of the four ORC configurations is shown in Fig. 4.5(b). The system cost rate decreases when T_{EVA} rises due to the declining capital cost rate and exergy destruction cost rate. The system cost rate for all configurations essentially achieves its lowest point at 370 K; however, after that point, the exergy loss cost rate rises, significantly raising the system cost rate. Further, Fig. 4.5(b) reveals that the Basic ORC has the highest system cost rate throughout the majority of the temperature range (350-400 K), whereas the RR-ORC has the lowest system cost rate for the temperature range of 363-386 K.

Effect of condenser temperature

The impact of condenser temperature (T_{COND}) on the exergy efficiency of the four ORC configurations is shown in Fig. 4.6(a). The exergy efficiency decreases as T_{COND} increases because the net ORC power declines while the flue gas exergy drop at the VG is mostly unchanged. The exergy efficiency of the Basic ORC, Recuperative ORC, Regenerative ORC, and RR-ORC drops by 5.40%, 5.55%, 5.68%,

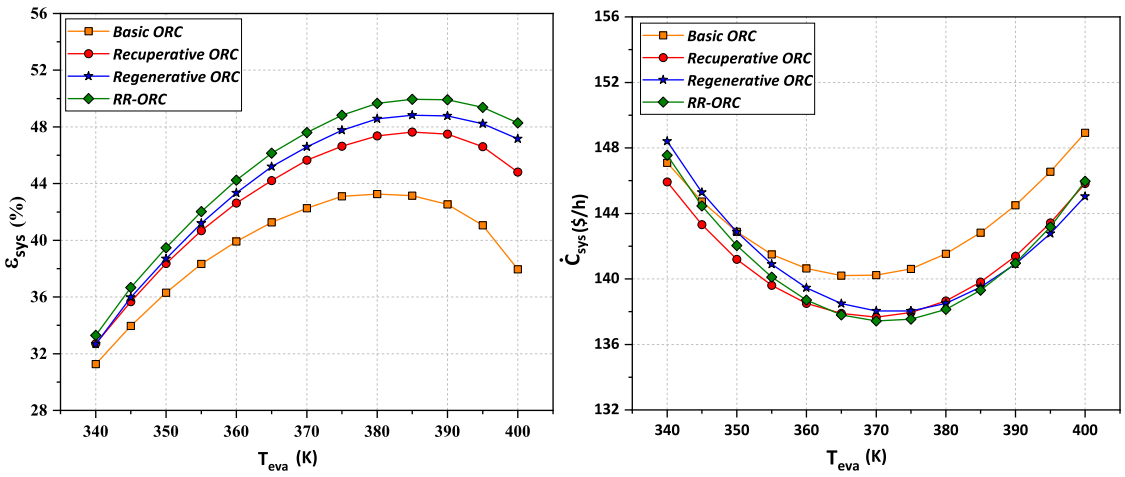

(a) Exergy efficiency (b) System cost rate

Fig. 4.5: Effect of evaporator temperature on the performance of ORCs.

and 6.02%, respectively, with a rise in T_{COND} from 304 K to 308 K. Also, in this case, the RR-ORC has the maximum exergy efficiency, whereas the Basic ORC has the lowest across the whole temperature range of the condenser.

Fig. 4.6(b) illustrates the impact of raising T_{COND} on the system cost rate for each of the four ORC configurations. Even though the overall capital cost rate slightly decreases as T_{COND} increases, the cost of exergy loss and destruction climbs dramatically, which causes the total system cost rate to increase. For low condenser temperatures (304–306.5 K), the system cost rate of the RR–ORC is the lowest; whereas, at T_{COND} over 306.5 K, the system cost rate of the Regenerative ORC is the lowest. It is also observed that the system cost rate of the Basic ORC is significantly high compared to the system cost rates of the other configurations through the range of the condenser temperature.

Effect of Pinch point temperature difference

Fig. 4.7(a) illustrates the impact of PPTD on the exergy efficiency of the four ORC layouts. Due to an increase in PPTD, the net power drops as the mass flow rate of R123 decreases. Furthermore, the fuel exergy at the VG decreases, but at a slower rate than the rate of reduction in work output. As a result, as PPTD increases from 281.15 K to 393.15 K, the exergy efficiency of the ORC configurations drops almost linearly. Additionally, the RR-ORC has the highest exergy efficiency across the entire PPTD range, while the Basic ORC has the lowest exergy efficiency.

Fig. 4.7(b) illustrates the impact of increasing PPTD on the system cost rate for each of the four ORC configurations. A rise in the cost rate associated with

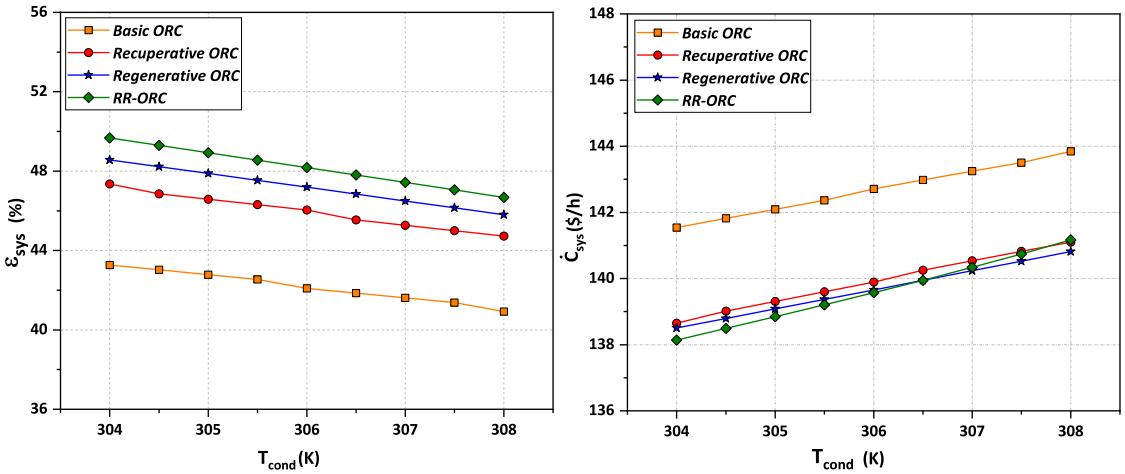

(a) Exergy efficiency (b) System cost rate

Fig. 4.6: Effect of condenser temperature on the performance of ORCs.

the exergy loss causes the system cost rate to rise linearly with PPTD. However, as PPTD rises, both the overall capital cost rate and the cost rate of exergy destruction decrease. The reason for an increase in the exergy loss cost rate is the increase in the flue gas temperature at the VG outlet. Additionally, it is important to note that the Basic ORC has the highest cost rate across the entire range of PPDT.

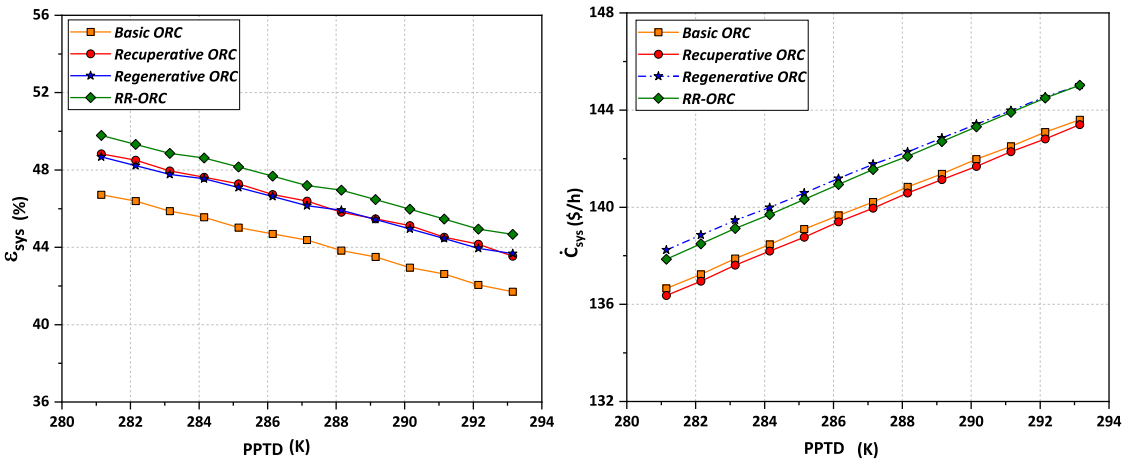

(a) Exergy efficiency (b) System cost rate

Fig. 4.7: Effect of PPTD on the performance of ORCs.

The parametric results suggest that the PPTD and T_{COND} are not highly responsive to the trade-off between the objective functions. However, in the case, of T_{EVA}, the trade-off between the exergy efficiency and the system cost rate for all four configurations is evident because the exergy efficiency is the maximum around 380 K while the system cost rate is minimum around 370 K.

4.4 Multi-objective optimization-based results

The set of optimal solutions in the form of a Pareto front obtained from the multi-objective optimization of each of the four ORC configurations is shown in Fig. 4.8. The goal of the multi-objective optimization, as previously stated, is to increase the exergy efficiency and lower the system cost rate by considering T_{EVA}, T_{COND}, and PPTD as the decision variables. The Pareto fronts are overlaid into the same objective space in Fig. 4.8 to compare the performance of the ORC configurations at their optimal conditions. It can be observed that the range of exergy efficiency is highest and the range of system cost rate is lowest for the Pareto front of the RR-ORC. Moreover, the Pareto front of the Basic ORC has the highest range of system cost rates and the lowest range of exergy efficiency. The Pareto fronts of the Regenerative ORC and Recuperative ORC are the next in order after the RR-ORC. Meanwhile, the best optimal solutions selected from the Pareto fronts of the four ORC layouts by using the TOPSIS decision-maker are highlighted in Figs. 4.9(a) to 4.9(d), respectively. The exergy efficiency and the system cost rate were given equal weights. It was accomplished by setting the weights (w_1, w_2) to 0.5.

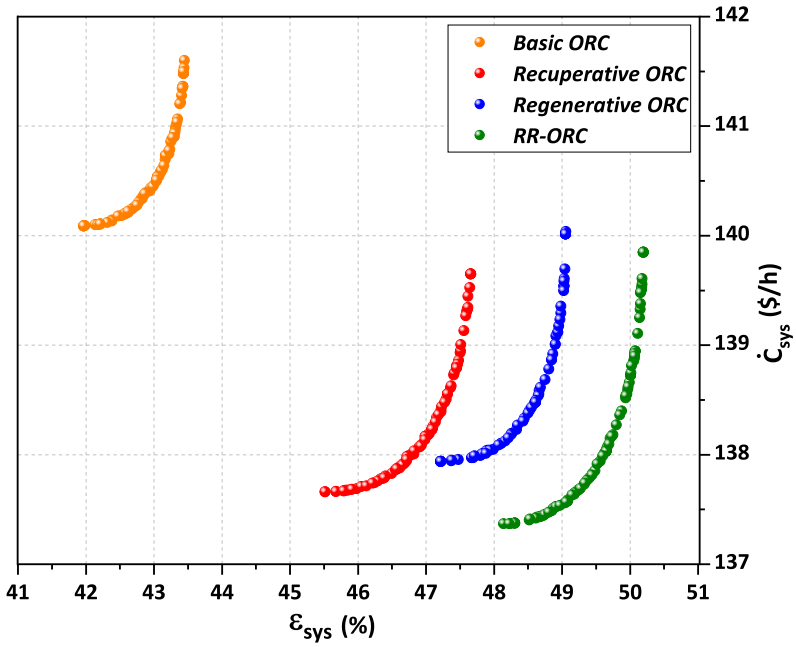

Fig. 4.8: The Pareto front obtained from the multi-objective optimization of the ORC configurations.

Table 4.9 displays the objective function values and corresponding decision variables for the four ORC configurations under optimal conditions. It can be observed that T_{EVA} for all configurations is selected in the range of 377.25 K to 382.27 K.

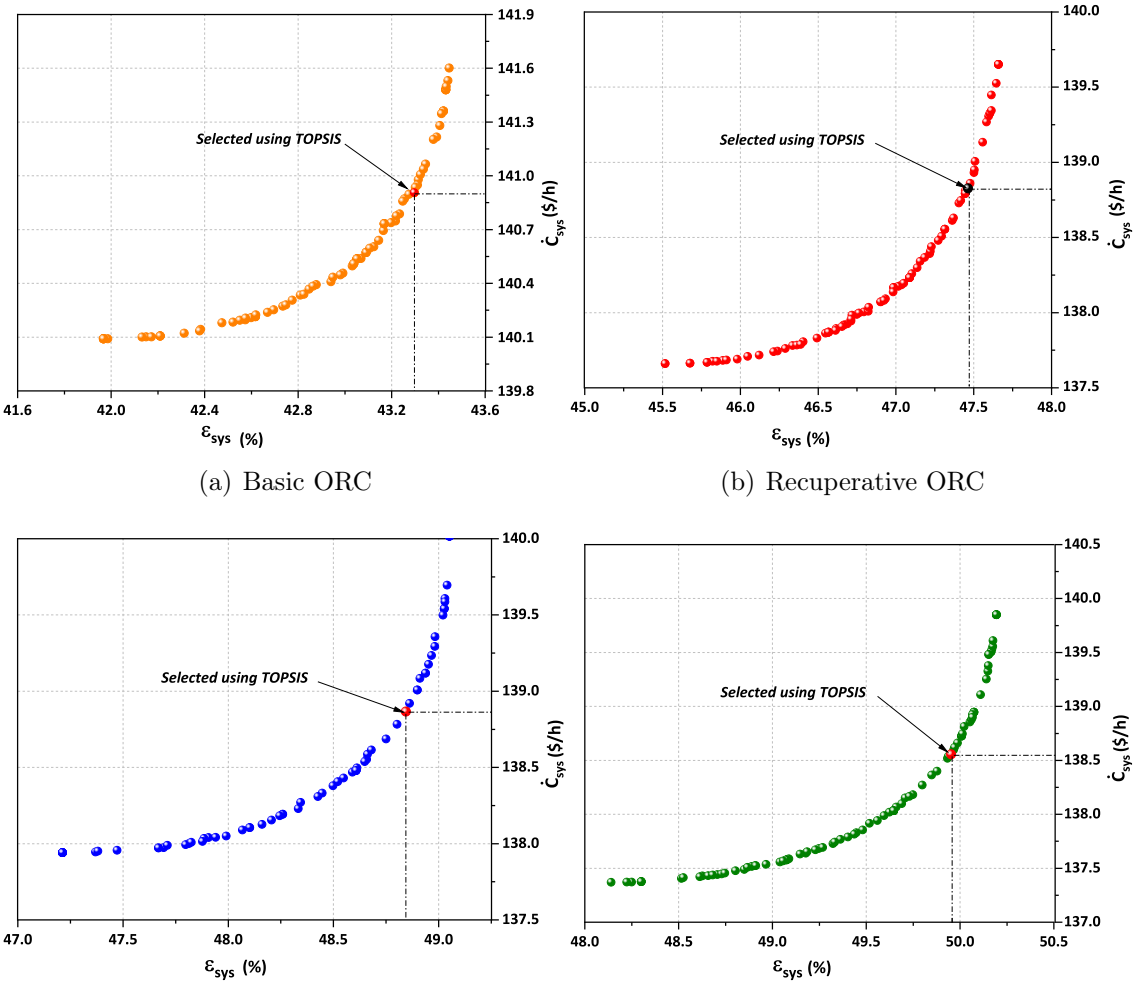

(a) Basic ORC

(b) Recuperative ORC

(c) Regenerative ORC

(d) RR-ORC

Fig. 4.9: The Pareto fronts highlighted with the final optimal solution.

Additionally, it was noted that T_{COND} for each case is the lower bound (304 K). Furthermore, it was noted that the Basic ORC has the highest PPTD while the Regenerative ORC and the RR-ORC have the lowest. Moreover, it is observed that the exergy efficiency and the system cost rate of the ORC configurations improve with each modification. The RR-ORC has the highest exergy efficiency of 49.95%, while the same is the lowest for the Basic ORC (43.31%). It indicates that with the use of IHE and the FH, the exergy efficiency of the RR-ORC improves by 15.33% over the Basic ORC. On the other hand, the Basic ORC has the highest system cost rate (140.95 $/h) while RR-ORC has the lowest system cost rate (138.58 $/h). In fact, the system cost rate of the RR-ORC is 1.68% lower than that of the Basic ORC.

The comprehensive energy, exergy and exergoeconomic results of the four ORCs at the optimal conditions are given in the following subsections.

Table 4.9: Optimal decision variables and objective function values of the four ORC configurations.

Parameters	Units	Basic ORC	Recuperative ORC	Regenerative ORC	RR-ORC
Objective functions					
ε_{sys}	%	43.31	47.46	48.84	49.95
$\dot{C}_{sys}$	\$/h	140.95	138.81	138.82	138.58
Decision variables					
T_{EVA}	K	377.25	380.93	382.27	382.18
T_{COND}	K	304.00	304.00	304.00	304.00
PPTD	K	289.35	284.95	281.65	281.65

4.4.1 Energy results

The state properties of the four ORC configurations are shown in Table 4.10. Additionally, Table 4.11 summarises the optimal energy-based performance criteria for the four configurations. As can be observed, the RR-ORC generates the maximum net power (825.21 kW), while the Basic ORC generates the lowest net power (710.21 kW). The net power of the Regenerative and Recuperative ORCs are intermediate to those of the RR-ORC and the Basic ORC. The optimal energy efficiencies of the ORC configurations likewise exhibit a similar pattern, with the RR-ORC showing the highest optimal energy efficiency (14.66%) and the Basic ORC being the lowest (12.76%). Therefore, it can be concluded with certainty that, in terms of energy output and energy efficiency, the RR-ORC is the most productive and efficient configuration, followed by the Regenerative ORC, Recuperative ORC, and Basic ORC.

4.4.2 Exergy results

The exergy-based results for the four ORC configurations under the corresponding optimum conditions are shown in Table 4.12. It is observed that the VG is the component with the highest exergy destruction rate in all four layouts, followed by the VT and the COND. The significant quantity of heat exchange between the flue gas and R123 with a finite temperature gradient is the cause of the high rate of exergy destruction at the VG. Further, it can be seen that the RR-ORC has the least overall exergy destruction rate (766.4 kW) whereas the Basic ORC has the highest overall exergy destruction rate (873.6 kW). Moreover, Table 4.12 shows that the FP (85.3%) and the VT (82.9%) are the most efficient components in the Basic ORC, while the COND and the VG perform poorly, with exergy efficiency of 38.2%

Table 4.10: The state properties, mass flow rate and the exergy rate at each state point of the ORC configurations.

Basic ORC					Recuperative ORC			
State	T (K)	P (kPa)	$\dot{m}$ (kg/s)	$\dot{E}$ (kW)	T (K)	P (kPa)	$\dot{m}$ (kg/s)	$\dot{E}$ (kW)
1	426.9	104.3	92.9	3736.9	426.9	104.3	92.9	3736.9
2	374.0	101.3	92.9	2096.7	374.1	101.3	92.9	2117.6
3	377.3	859.9	26.5	1002.9	380.9	931.1	27.5	1083.0
4	324.2	112.9	26.5	107.2	325.2	112.9	27.5	113.1
5	304.0	112.9	26.5	1.7	306.5	112.9	27.5	92.5
6	304.4	859.9	26.5	15.4	304.0	112.9	27.5	1.8
7	298.2	101.3	232.2	0.0	304.4	931.1	27.5	17.4
8	303.2	101.3	232.2	40.3	317.6	931.1	27.5	33.0
9	–	–	–	–	298.2	101.3	224.9	0.0
10	–	–	–	–	303.2	101.3	224.9	39.0
Regenerative ORC					RR-ORC			
State	T (K)	P (kPa)	$\dot{m}$ (kg/s)	$\dot{E}$ (kW)	T (K)	P (kPa)	$\dot{m}$ (kg/s)	$\dot{E}$ (kW)
1	426.9	104.3	92.9	3736.9	426.9	104.3	92.9	3736.9
2	373.5	101.3	92.9	2086.6	373.5	101.3	92.9	2084.8
3	382.3	958.0	29.3	1167.8	382.2	956.2	29.38	1169.1
4	340.6	220.0	3.2	49.0	340.5	220.0	1.16	17.9
5	325.3	112.9	26.1	107.4	325.3	112.9	28.21	115.9
6	304.0	112.9	26.1	1.7	306.2	112.9	28.21	94.6
7	304.1	220.0	26.1	3.7	304.0	112.9	28.21	1.9
8	324.3	220.0	29.3	35.4	304.1	220.0	28.21	4.0
9	324.7	958.0	29.3	51.2	317.5	220.0	28.21	19.9
10	298.2	101.3	230.1	0.0	324.3	220.0	29.38	35.5
11	303.2	101.3	230.1	39.9	324.7	956.2	29.38	51.2
12	–	–	–	–	298.2	101.3	230.0	0.0
13	–	–	–	–	303.2	101.3	230.0	39.9

Table 4.11: Energy-based performance parameters of the four ORC configurations.

Parameters	Units	Basic ORC	Recuperative ORC	Regenerative ORC	RR-ORC
$\dot{W}_{VT}$	kW	726.27	786.72	826.44	845.90
$\dot{W}_{FP-I}$	kW	16.05	18.29	2.27	2.45
$\dot{W}_{FP-II}$	kW	-	-	18.24	18.23
$\dot{W}_{net}$	kW	710.21	768.43	805.93	825.21
η_{sys}	%	12.76	14.07	14.34	14.66

and 60.2%, respectively. As a result of preheating R123 before feeding it to the VG, the exergy efficiencies of the COND and the VG rise in the Recuperative ORC to 51.7% and 64.8%, respectively. The exergy efficiency of the VG rises to 67.3% in the Regenerative ORC as well, because of the employment of the FH, but the exergy

efficiency of the COND does not change. The FH's performance in the RR-ORC is rather acceptable, with a corresponding exergy efficiency of 94.0%, and it is also found that the exergy efficiency of all common components in the RR-ORC and the Regenerative ORC are nearly identical. The exergy efficiency of the IHE, which was 64.8% in the Recuperative ORC, increased to 74.6% in the RR-ORC. Moreover, the RR-ORC has the highest overall system exergy efficiency (49.95%) while the Basic ORC has the lowest (43.31%). The Regenerative and Recuperative ORCs both have better overall exergy efficiency than the Basic ORC, while they are marginally less efficient than the RR-ORC. Meanwhile, the exergy carried away by the flue gas at the exit of VG is referred to as exergy loss ($\dot{E}_2$) [5] in this study. The magnitude of the exergy loss depends on temperature, mass flow rate, and the flue gas composition at the VG exit. The flue gas mass flow rate is the same in all four ORC layouts, however, the flue gas temperature at the VG output varies. Hence, the exergy loss rates are also different for different layouts. The RR-ORC layout has the lowest exergy loss of 2084.8 kW owing to lowest flue gas exit temperature.

4.4.3 Exergoeconomic results

Table 4.13 presents the cost flow rate and the cost per unit exergy at each state point of the ORC configurations. Further, Table 4.12 presents a summary of the exergoeconomic results for each component of the ORC configurations. As can be seen, in all four ORC configurations, VG contributes the highest exergy destruction cost rate compared to the other components. In fact, VG accounts for almost 63% and 61% of the overall exergy destruction cost rate in the Basic and Recuperative ORC, respectively. However, in the Regenerative and RR-ORC, the percentage share of the VG's exergy destruction cost rate reduces to 57.4% and 59.1%, respectively. Meanwhile, the VT has the highest capital cost rate among all the components of the ORC layouts. It is also essential to note that the capital cost rate of VT has the highest value in the RR-ORC (14.62 \$/h) and the lowest value in the Basic ORC (13.14 \$/h). The PEC_k for the components of the ORC layouts are presented in Table A.1 (refer to Appendix).

Table 4.12 also presents the $\dot{C}_D + \dot{Z}$ values for each component of the ORC layouts. According to Ref. [5], a component in a given system that has the highest $\dot{C}_D + \dot{Z}$ value is the most critical component as per exergoeconomic viewpoint. Based on this fact, it can be inferred that the VG needs special consideration in the Basic ORC owing to the highest $\dot{C}_D + \dot{Z}$ value of 26.77 \$/h. However, VT is the most critical component in the Recuperative ORC, Regenerative ORC and RR-ORC

Table 4.12: Exergy and Exergoeconomic parameters obtained at the optimal conditions of the ORC configurations.

Components	$\dot{E}_D$ (kW)	ε (%)	$\dot{C}_D$ (\$/h)	$\dot{Z}$ (\$/h)	$\dot{C}_D + \dot{Z}$ (\$/h)	r_k (%)	f (%)
Basic ORC							
VG	652.7	60.2	26.20	0.57	26.77	67.6	2.14
VT	153.4	82.9	10.51	13.14	23.65	46.5	55.56
COND	65.1	38.2	4.46	1.07	5.53	200.8	19.40
FP	2.4	85.3	0.24	0.49	0.75	54.03	68.14
Total	873.66	43.31	41.41	15.37	56.78	-	10.90
Recuperative ORC							
VG	569.4	64.8	22.86	0.58	23.44	55.6	2.48
VT	164.8	83	10.60	13.90	24.5	44.1	56.74
COND	51.7	43	3.32	1.12	4.44	170.6	25.17
FP	2.7	85.3	0.25	0.64	0.89	54.8	71.47
IHE	5.1	64.8	0.33	0.23	0.56	53.3	41.73
Total	793.7	47.46	37.35	16.47	53.82	-	11.86
Regenerative ORC							
VG	533.8	67.7	21.4	0.59	21.96	49.1	2.7
VT	164.4	83.7	10.3	14.39	24.69	46.4	58.2
COND	65.8	37.7	4.1	1.19	5.29	212.3	22.3
FP-I	0.3	85.3	0.0	0.15	0.15	98.5	82.5
FP-II	2.5	86.2	0.2	0.64	0.84	59.9	73.3
FH	17.3	67.3	1.2	0.82	2.02	83.1	82.9
Total	784.1	48.84	37.3	17.77	55.07	-	12.79
RR-ORC							
VG	534.3	67.7	21.4	0.59	21.99	49.1	2.69
VT	168.7	83.7	10.6	14.62	25.22	46.2	57.91
COND	52.8	43	3.3	1.19	4.49	179.9	26.37
FP-I	0.4	85.3	0.0	0.15	0.15	96.7	82.16
FP-II	2.5	86.2	0.2	0.64	0.84	59.9	73.33
FH	2.3	94	0.2	1.24	1.44	47.5	85.32
IHE	5.4	74.6	0.3	0.24	0.54	57.5	40.69
Total	766.4	49.95	36.20	18.70	54.9	-	13.47

with the respective highest $\dot{C}_D + \dot{Z}$ values of 24.5, 24.69 and 25.22 \$/h. Moreover, a component with a large value of relative cost difference signifies a higher chance of improving the cost-effectiveness of the overall system if the costs of that specific component are reduced. The COND is the component with a notably large relative cost difference in each of the ORC configurations. In fact, the relative cost difference is inversely correlated with exergy efficiency [12]. Therefore, the cost-effectiveness of the overall system could be improved by reducing the exergy or non-exergy re-

lated costs of the COND. Additionally, Table 4.12 demonstrates that among all the components in all four configurations, VG has the lowest exergoeconomic factor. In both the Basic and Recuperative ORCs, the FP exhibits the highest exergoeconomic factor. The FH, on the other hand, shows the largest exergoeconomic factor in both the Regenerative ORC and RR-ORC. The low exergoeconomic factor of VG implies that the cost rate related to exergy destruction is heavily dominated in comparison to the capital cost rate. Similarly, a relatively high value of the exergoeconomic factor in the case of FP and FH, indicates that the capital cost rate is significant compared to the cost rates of exergy destruction and exergy loss.

Table 4.13 also demonstrates that RR-ORC has the lowest overall exergy destruction cost rate (36.20 \$/h) while the Basic ORC has the highest (41.41 \$/h). The total exergy destruction cost rates of the Recuperative and Regenerative ORCs are 37.35 \$/h and 37.3 \$/h, respectively. Meanwhile, the RR-ORC has the highest total capital cost rate (18.70 \$/h), followed by the Regenerative ORC (17.77 \$/h), the Recuperative ORC (16.47 \$/h), and the Basic ORC (15.37 \$/h). The total capital cost rate is the highest for the RR-ORC among the four layouts since it has the most components in its system configuration. The increase in the total capital cost rate from the Basic ORC to the RR-ORC can be partially attributed to an increase in the capital cost rates of the VT, which in fact increases owing to the increase in power output. Besides, the capital cost rate of the FH, which is an additional component in the RR-ORC, is also relatively high compared to its counterpart in the Regenerative ORC. Further, it is found that the cost rate of exergy loss exhibits the same pattern as the rate of exergy loss, which is reasonable considering that the cost rate of exergy loss is just a function of the exergy loss rate. The RR-ORC and the Recuperative ORC were previously found to have the maximum and minimum exergy loss rates, and as a result, these configurations also have the minimum and maximum exergy loss cost rates of 83.68 \$/h and 84.16 \$/h, respectively. Moreover, it is observed that the RR-ORC has a maximum exergoeconomic factor of 13.47%, indicating that exergy destruction and exergy loss cost rates account for 86.53% of the total cost rates, while capital cost rate makes up the remaining 13.47%. The Basic ORC has the lowest overall exergoeconomic factor, and the overall exergoeconomic factors of the other two ORC configurations are intermediate to those of the Basic and RR-ORC.

Table 4.13: The cost flow rate and the cost per unit exergy at each state point of the ORC configurations.

	Basic ORC		Recuperative ORC		Regenerative ORC		RR-ORC	
State	$\dot{C}$ (\$/h)	c (\$/GJ)	$\dot{C}$ (\$/h)	c (\$/GJ)	$\dot{C}$ (\$/h)	c (\$/GJ)	$\dot{C}$ (\$/h)	c (\$/GJ)
1	150	11.1	150	11.1	150	11.1	150	11.1
2	84.2	11.1	85	11.1	83.8	11.1	83.7	11.1
3	68.7	19	69.6	17.9	73.5	17.5	73.7	17.5
4	7.3	19	7.3	17.9	3.1	17.5	1.1	17.5
5	0.1	19	5.9	17.9	6.8	17.5	7.3	17.5
6	2.3	41.6	0.1	17.9	0.1	17.5	6	17.5
7	0	0	2.5	39.7	0.5	35.1	0.1	17.5
8	8.3	57.3	4.1	34.1	4.4	34.3	0.5	34.9
9	72.9	27.9	0	0	6.7	36.3	2.1	29
10	1.6	27.9	6.9	49.5	0	0	4.4	34.8
11	-	-	74.5	26.3	7.8	54.6	6.8	36.7
12	-	-	1.7	26.3	76.2	25.6	0	0
13	-	-	-	-	0.2	25.6	7	49
14	-	-	-	-	1.7	25.6	78	25.6
15	-	-	-	-	-	-	0.2	25.6
16	-	-	-	-	-	-	1.7	25.6

4.5 Summary

In this chapter, four ORC configurations (Basic ORC, Recuperative ORC, Regenerative ORC, and RR-ORC) are optimized by using PESA-II, considering the exergy efficiency and the system cost rate as the objective functions. A parametric analysis is also performed to obtain a preliminary idea about the effect of decision variables on the objective functions. Then to choose the best optimal solutions for each of the four ORC configurations, multi-criteria decision analysis is carried out on the Pareto fronts using the TOPSIS decision-maker. The energy, exergy, and exergoeconomic-based performance parameters are evaluated at the optimal conditions to compare the performance of the four configurations. The analysis reveals that among the four systems, the RR-ORC is the most efficient and cost-effective configuration and hence, the use of RR-ORC in preference to the other three is recommended. The other main findings obtained from this optimization and comparative study are highlighted below.

- It is found that the Basic ORC, Recuperative ORC, Regenerative ORC, and RR-ORC configurations have an increasing order of power and efficiency and a decreasing order of exergy destruction.

- The system cost rates for the Recuperative, Regenerative, and RR-ORC are more or less the same, however, the system cost rate of the RR-ORC is the lowest. Furthermore, these three configurations have lower system cost rates than the Basic ORC.

- The RR-ORC has the highest energy and exergy efficiencies of 14.66% and 49.95%, respectively, with a maximum net power output of 825.21 kW. The RR-ORC also has the minimum exergy destruction and system cost rates of 766.4 kW and 138.58 $/h, respectively.

- The net power, energy and exergy efficiencies of the RR-ORC are respectively 16.19%, 14.89% and 15.33% higher while the exergy destruction rate and system cost rate are 12.28% and 1.68% lower than those of the Basic ORC.

- The most critical component based on the exergoeconomic viewpoint is the VG in the Basic ORC, however, VT is the most critical component in the Recuperative ORC, Regenerative ORC and RR-ORC.

- In all four ORC configurations, the cost rate of exergy loss constitutes, on average, 60% of the overall system cost rate.

This study suggests that to increase the overall performance of the combined power and cooling systems presented in Chapter 3, the Recuperative ORC included in the system should be replaced with more efficient and economical RR-ORC.

Bibliography

[1] Ahmadi, P. and Dincer, I. Thermodynamic and exergoenvironmental analyses, and multi-objective optimization of a gas turbine power plant. *Applied Thermal Engineering*, 31(14-15):2529–2540, 2011.

[2] Ahmadi, P., Dincer, I., and Rosen, M. A. Exergy, exergoeconomic and environmental analyses and evolutionary algorithm based multi-objective optimization of combined cycle power plants. *Energy*, 36(10):5886–5898, 2011.

[3] Anvari, S., Jafarmadar, S., and Khalilarya, S. Proposal of a combined heat and power plant hybridized with regeneration organic Rankine cycle: Energy-Exergy evaluation. *Energy Conversion and Management*, 122:357–365, 2016.

[4] Anvari, S., Taghavifar, H., and Parvishi, A. Thermo- economical consideration of Regenerative organic Rankine cycle coupling with the absorption chiller systems incorporated in the trigeneration system. *Energy Conversion and Management*, 148:317–329, 2017.

[5] Bejan, Adrian, George Tsatsaronis and Moran., M. J. *Thermal design and optimization*. John Wiley Sons, New York, 1995.

[6] Björck, Å. *Numerical methods in matrix computations*, volume 59. Springer, 2015.

[7] Çelikbilek, Y. and Tüysüz, F. An in-depth review of theory of the TOPSIS method: An experimental analysis. *Journal of Management Analytics*, 7(2): 281–300, 2020.

[8] Corne, D. W., Knowles, J. D., and Oates, M. J. The pareto envelope-based selection algorithm for multiobjective optimization. In Schoenauer, M., Deb, K., Rudolph, G., Yao, X., Lutton, E., Merelo, J. J., and Schwefel, H.-P., editors, *Parallel Problem Solving from Nature PPSN VI*, pages 839–848, Berlin, Heidelberg, 2000. Springer Berlin Heidelberg.

[9] Corne, D. W., Jerram, N. R., Knowles, J. D., and Oates, M. J. PESA-II: Region-based Selection in Evolutionary Multiobjective Optimization. In Spector et al., L., editor, *Proc. 3rd Annual Conference on Genetic and Evolutionary Computation*, pages 283–290, San Francisco, CA, United States, 2001.

[10] Ebrahimi-Moghadam, A., Farzaneh-Gord, M., Jabari Moghadam, A., Abu-Hamdeh, N. H., Lasemi, M. A., Arabkoohsar, A., and Alimoradi, A. Design and multi-criteria optimisation of a trigeneration district energy system based on gas turbine, Kalina, and ejector cycles: Exergoeconomic and exergoenvironmental evaluation. *Energy Conversion and Management*, 227:113581, 2021.

[11] Heidarnejad, P., Genceli, H., Asker, M., and Khanmohammadi, S. A comprehensive approach for optimizing a biomass assisted geothermal power plant with freshwater production: Techno-economic and environmental evaluation. *Energy Conversion and Management*, 226:113514, 2020.

[12] Khaljani, M., Khoshbakhti Saray, R., and Bahlouli, K. Comprehensive analysis of energy, exergy and exergo-economic of cogeneration of heat and power in a combined gas turbine and organic Rankine cycle. *Energy Conversion and Management*, 97:154–165, 2015.

[13] Khanmohammadi, S. and Azimian, A. R. Exergoeconomic Evaluation of a Two-Pressure Level Fired Combined-Cycle Power Plant. *Journal of Energy Engineering*, 141(3):04014014, 2015.

[14] Kianfard, H., Khalilarya, S., and Jafarmadar, S. Exergy and exergoeconomic evaluation of hydrogen and distilled water production via combination of PEM electrolyzer, RO desalination unit and geothermal driven dual fluid ORC. *Energy Conversion and Management*, 177:339–349, 2018.

[15] Köse, Ö., Koç, Y., and Yağlı, H. Energy, exergy, economy and environmental (4E) analysis and optimization of single, dual and triple configurations of the power systems: Rankine Cycle/Kalina Cycle, driven by a gas turbine. *Energy Conversion and Management*, 227:113604, 2021.

[16] Lemmon E, Huber M, M. M. NIST Standard Reference Database 23, Reference Fluid Thermodynamic and Transport Properties (REFPROP), version 9.0, National Institute of Standards and Technology, R1234yf. fld file dated December 22 (2010). Technical report, NIST. URL `https://www.nist.gov/system/files/documents/srd/REFPROP8_manua3.htm`.

[17] Nami, H. and Akrami, E. Analysis of a gas turbine based hybrid system by utilizing energy, exergy and exergoeconomic methodologies for steam, power and hydrogen production. *Energy Conversion and Management*, 143:326–337, 2017.

[18] Nondy, J. and Gogoi, T. K. Performance comparison of multi-objective evolutionary algorithms for exergetic and exergoenvironomic optimization of a benchmark combined heat and power system. *Energy*, 233:121135, 2021.

[19] Safarian, S. and Aramoun, F. Energy and exergy assessments of modified Organic Rankine Cycles (ORCs). *Energy Reports*, 1:1–7, 2015.

[20] Sayyaadi, H. Multi-objective approach in thermoenvironomic optimization of a benchmark cogeneration system. *Applied Energy*, 86(6):867–879, 2009.

[21] Towler, G. and Sinnott, R. *Chemical engineering design: principles, practice and economics of plant and process design*. Butterworth-Heinemann, 2021.

[22] Yağlı, H., Koç, Y., and Kalay, H. Optimisation and exergy analysis of an organic Rankine cycle (ORC) used as a bottoming cycle in a cogeneration system producing steam and power. *Sustainable Energy Technologies and Assessments*, 44:100985, 2021.